

UC San Diego

UC San Diego Previously Published Works

Title

Nonlinear 3D projection printing of concave hydrogel microstructures for long-term multicellular spheroid and embryoid body culture

Permalink

<https://escholarship.org/uc/item/06f893g4>

Journal

Lab on a Chip, 15(11)

ISSN

1473-0197

Authors

Hribar, KC
Finlay, D
Ma, X
[et al.](#)

Publication Date

2015-06-07

DOI

10.1039/c5lc00159e

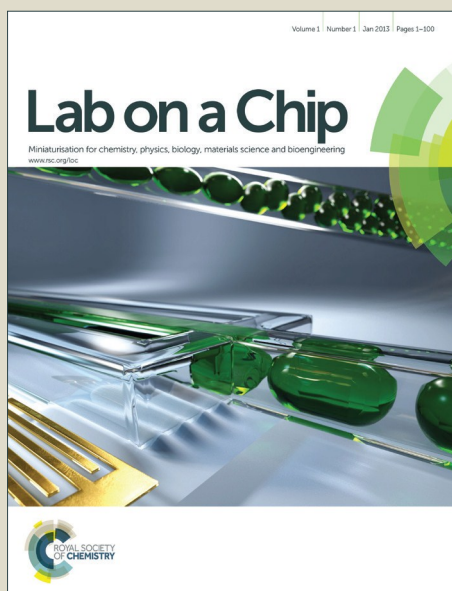
Peer reviewed

Lab on a Chip

Accepted Manuscript



This article can be cited before page numbers have been issued, to do this please use: K. C. Hribar, D. Finlay, X. Ma, X. Qu, M. G. Ondeck, P. H. Chung, F. Zanella, A. J. Engler, F. Sheikh, K. Vuori and S. Chen, *Lab Chip*, 2015, DOI: 10.1039/C5LC00159E.



This is an *Accepted Manuscript*, which has been through the Royal Society of Chemistry peer review process and has been accepted for publication.

Accepted Manuscripts are published online shortly after acceptance, before technical editing, formatting and proof reading. Using this free service, authors can make their results available to the community, in citable form, before we publish the edited article. We will replace this *Accepted Manuscript* with the edited and formatted *Advance Article* as soon as it is available.

You can find more information about *Accepted Manuscripts* in the [Information for Authors](#).

Please note that technical editing may introduce minor changes to the text and/or graphics, which may alter content. The journal's standard [Terms & Conditions](#) and the [Ethical guidelines](#) still apply. In no event shall the Royal Society of Chemistry be held responsible for any errors or omissions in this *Accepted Manuscript* or any consequences arising from the use of any information it contains.

ARTICLE

Nonlinear 3D Projection Printing of Concave Hydrogel Microstructures for Long-Term Multicellular Spheroid and Embryoid Body Culture

K.C Hribar,^a D. Finlay,^b X. Ma,^c X. Qu,^a M. G. Ondeck,^d P. H. Chung,^a F. Zanella,^e A. J. Engler,^{c,f} F. Sheikh,^e K. Vuori,^b and S. Chen^{*a}

Received
Accepted

DOI: 10.1039/x0xx00000x

www.rsc.org/

Long-term culture and monitoring of individual multicellular spheroids and embryoid bodies (EBs) remains a challenge for *in vitro* cell propagation. Here, we used a continuous 3D projection printing approach –with an important modification of nonlinear exposure – to generate concave hydrogel microstructures that permit spheroid growth and long-term maintenance, without the need for spheroid transfer. Breast cancer spheroids grown to 10 d in the concave structures showed hypoxic cores and signs of necrosis using immunofluorescent and histochemical staining, key features of the tumor microenvironment *in vivo*. EBs consisting of induced pluripotent stem cells (iPSCs) grown on the hydrogels demonstrated narrow size distribution and undifferentiated markers at 3 d, followed by signs of differentiation by the presence of cavities and staining of the three germ layers at 10 d. These findings demonstrate a new method for long-term (e.g. beyond spheroid formation at day 2, and with media exchange) 3D cell culture that should be able to assist in cancer spheroid studies as well as embryogenesis and patient-derived disease modeling with iPSC EBs.

A. Introduction

In the fields of bioengineering and cell biology, three-dimensional (3D) cell culture provides a means to more accurately resemble the physiological *in vivo* environment for preclinical studies (e.g. drug screening, cellular assays).^[1-3] Specifically, multicellular spheroids have been extensively used for studying embryogenesis in the form of embryoid bodies (EBs),^[4-6] adult tissue growth and organogenesis,^[7,8] cancer progression and liver toxicity.^[9,10] To date, technologies that generate multicellular spheroids are limited in culture duration (requiring spheroid transfer), optical clarity issues for imaging, or broad size distributions.

The hanging-drop method is a commercially available technique that has been extensively utilized in spheroid culture, yet this process is labor intensive due to the need for spheroid transfer and sometimes lacks reproducibility.^[11] Micromolding and photolithography have been used to create microwells made of PDMS,^[12,13] or hydrogels such as poly(ethylene glycol) (PEG)^[14,15] and agarose.^[16] But these technologies sometimes require multiple labor steps and produce microwells with limited optical transparency for imaging, protein

adsorption issues, size restrictions or sample loss with media exchange, thus resorting to spheroid transfer to another plate.

Here, we created hydrogel microstructures made of photocrosslinkable PEGDA with gradual concave topographies that are optically clear and can be utilized for long-term (e.g. with media-exchange, for durations beyond 2-3 days) cell spheroid culture. PEG is an FDA approved biomaterial and often utilized in cell culture for its low immunogenicity, minimal protein adsorption, lack of adhesive peptides (which in turn limits cell-material interaction and promotes cell aggregation), as well as optical clarity.^[17] The structures are fabricated with a 3D projection printer that uses nonlinear UV light exposure. We demonstrate their feasibility for spheroid culture in two distinct models – breast cancer spheroids and induced pluripotent stem cells (iPSC) EBs. In the breast cancer model, we grow the spheroids to 10 d, noting size changes and staining of hypoxia and necrosis, important markers in tumor progression.^[9] Next, we use the platform to generate EBs of iPSCs. iPSCs have become a desirable cell type as they are autologous (patient-derived) by nature and thus have the potential to be used in a multitude of patient-specific *in vitro* models and therapies. We show tight uniformity in EB size

after 3 d, with important undifferentiated markers expressed. Expanding the culture to 10 d, we witness the EBs' spontaneous differentiation into the three germ layers, as evidenced by immunofluorescent staining. Importantly, EBs remained within the concave hydrogels during the entire process. This platform opens the door for more biological models to be developed of many cell types, including, but not limited to, cancer, embryogenesis, and patient-derived disease models using iPSCs.

Experimental

Continuous 3D Printing Using Nonlinear Optical Projection

This 3D printing protocol was adapted from a previously described technology,^[18] with the modification of nonlinear UV light exposure for generating concave structures. Prepolymer solution consisting of 20% poly(ethylene glycol) diacrylate (PEGDA) (MW 700, Sigma), 0.05% Irgacure 2959 (Ciba) in phosphate buffer saline (PBS) was administered between two glass slides and exposed to 10 mW/cm² UV light source (Omnicure S2000, 365 nm) using dynamic optical projection stereolithography setup. On the computer, a gradient pattern was designed in Adobe Photoshop and converted to a grayscale image. The image was then processed through in-house software and z-sliced into a series of transverse planes, according to the grayscale intensity of each pixel. These planes were successively and continuously fed onto the DMD chip as optical masks to be projected onto the prepolymer solution. Nonlinear exposure time was controlled by the following equation:

$$\text{Total exposure time} = T_0 + T_0 \cdot (1 + L_i \cdot A_2)^2 \quad (1)$$

where T_0 is the exposure time for the base layer, L_i is the layer number, and A_2 is the nonlinear factor. Total exposure time is the aggregate exposure for all the layers. Based on the exposure time and inputted height, the software adjusts the speed of the automated stage. In this case, the z-height for all structures was held constant at 500 μm . Hydrogels were polymerized onto glass coverslips pretreated with the chemical modification of 3-(Trimethoxysilyl)-Propyl Methacrylate (TMSPPMA). After fabrication, the hydrogels were washed three times in PBS over the course of two days.

Atomic Force Microscopy

Stiffness of the hydrogels was confirmed by atomic force microscopy (AFM; MFP3D, Asylum Research) as detailed previously.^[18,20] Briefly, a pyramidal probe, 0.08 N/m spring constant with a 35° half angle (PNP-TR20, Nanoworld), was used to indent the substrate. The probe indentation velocity was fixed at 2 $\mu\text{m/s}$ with the trigger force of 2 nN. Elastic modulus maps were determined by the Hertz cone model with a sample Poisson ratio of 0.5 fit over a range of 10%-90% indentation force.²⁷ AFM software (Igor pro 6.22) was applied to generate the stiffness.

Scanning Electron Microscopy (SEM)

Hydrogel samples were dehydrated using increasing amounts of ethanol:water (i.e. 20% ethanol, 30%, and so on) until they were submerged in 100% ethanol and dried via critical point drying (Tousimis AutoSamdri 815A). Samples were then

sputter coated with iridium and imaged using an FEI SFEG Ultra-High Resolution SEM.

Breast Cancer Cell culture and Hydrogel Seeding

BT474 breast cancer cells were used for tumor spheroid studies. BT474 cells were obtained from ATCC and were maintained in RPMI-1640 media supplemented with 10% (v/v) fetal bovine serum (FBS), penicillin/streptomycin/L-glutamine, and Fungizone (Omega Scientific Inc.). Hydrogels were sterilized under UV light, and BT474 cells were seeded into the wells at the concentrations of 250K mL⁻¹ (LOW) and 750K mL⁻¹ (HIGH).

BT474 Spheroid Imaging, Sectioning, and Analysis

Brightfield images of cancer spheroids were taken at various timepoints using a Leica Fluorescence Microscope, and a live/dead fluorescence assay (calcein AM/ethidium homodimer) was performed at day 10 to qualitatively assess cell viability. Spheroid size was quantified using ImageJ software. Spheroids also grown to day 10 were fixed in 4% paraformaldehyde and cryosectioned at 20 μm thickness. Sections were stained for HIF-1 α (1:50 HIF-1 α mouse mAb, Novus Biologicals), a hypoxia marker, and DAPI, a nuclear stain, and H&E staining was also performed.

Integration-free Human Induced Pluripotent Stem Cells (iPSCs) Generation

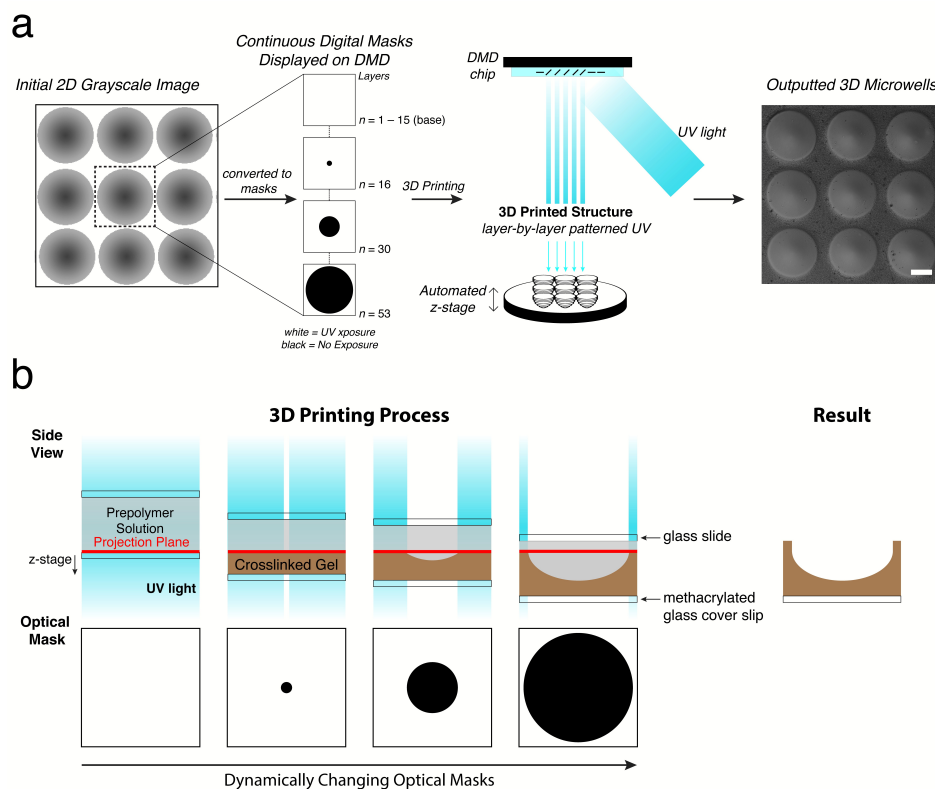
Human perinatal foreskin fibroblasts (BJ, ATCC) and human adult dermal fibroblasts (HDF, Cell Applications) were maintained in DMEM (Corning) supplemented with 10% FBS (Tissue Culture Biologicals) and Antibiotics/Antimycotic (Corning) in a 37°C, 5%CO₂ incubator. Cells were passaged at a ratio of 1:6 every 3-5 days by 0.25% Trypsin-EDTA (Corning) before reprogramming. To prepare for reprogramming, fibroblasts were seeded at a density of 2 x 10⁵ cells/well in 6-well plates, and allowed to attach and spread for 48h. Reprogramming was performed following the instructions in a Sendai virus-based Cyto Tune kit (Life technologies) for the delivery of four factors Oct4, Sox2, Klf4 and c-Myc.

Human iPSC Culture and EB Formation

Following successful reprogramming, growth factor reduced Matrigel (BD Biosciences, NJ, USA) was used as the substrate for the maintenance of the iPSCs culture in serum- and feeder-free conditioned medium (StemPro®, Life Technologies) following the manufacturer's instructions. Cells were split at a ratio of 1:6 every 3-4 days by Versene (Life Technologies) before experiments.

Similar to our cancer cell seeding protocol, hydrogels were sterilized under UV for 1 hour. Human iPSCs at 70–80% confluency were detached by Accutase (Innovative Cell Technologies) and resuspended in regular culture medium with 5 μM ROCK inhibitor Y27632 (Stemgent). Cells were seeded at concentrations of 100 k or 400 k mL⁻¹ into each of the well of a 24-well plate, which had an individual hydrogel array construct. The plates were spun at a speed of 50 g for 3 minutes and then incubated in a 37°C, 5% CO₂ incubator. Maintenance medium was replaced everyday. EBs formed spontaneously within the center of each concave hydrogel structure, and were monitored and imaged using a Leica DIC microscope. Image analysis (e.g. EB diameter size) was performed on imageJ software.

Figure 1. (a) Detailed schematic of the continuous 3D printing process. A grayscale image is divided into a series of digital masks (53 layers in total, 15 “base” layers where the entire structure is exposed to UV light). A white mask denotes a layer that is completely exposed to UV light, while black in the mask describes areas of no exposure for any given layer. Due to the gradient pattern in the grayscale image, the center of each concave structure receives the least amount of total UV exposure. The outputted structure is displayed on the right (scaled bar = 200 μm). (b) Cross-sectional schematic of the 3D printing process over the course of all 53 layers. All scale bars = 200 μm .



EB Immunofluorescence Staining

Embryoid bodies (EBs) were fixed within the hydrogels in 4% paraformaldehyde in PBS three days following seeding. They were subsequently permeabilized with 0.1% Triton X-100 in PBS and incubated with antibodies against Oct4 (Cell Signaling Technology) and Nanog (Cell Signaling Technology) followed by fluorophore-conjugated anti-IgG antibodies. DAPI (Invitrogen) nucleus counterstain was also performed. For differentiation studies, EBs were grown in the same manner on the concave hydrogels at varying concentrations (100 or 400 k cells mL^{-1}) for 10 days, followed by fixing and immunostaining with biomarkers for the three germ layers: SOX-1 for ectoderm, SOX-17 for endoderm, and Brachyury for mesoderm (R&D Systems). Images were taken using a Leica fluorescence microscope and an Olympus confocal microscope.

Results and discussion

Concave hydrogel microstructures for spheroid culture were fabricated using a light-based, continuous 3D projection printing technology adapted with nonlinear UV light exposure. (Figure 1a).^[18,21] A 2D image of a gradient circle pattern is converted to a series of layer slices (53 layers in total) based on its grayscale intensity at each pixel (Figure 1a). Each layer represents a cross-sectional image in the series in proportion to the height of the structure (500 μm). The series is then fed to the digital micromirror device (DMD) for UV projection onto the photocurable prepolymer solution – in this case, 20% (w/v) poly(ethylene glycol) (PEG) diacrylate – in a continuous fashion. Importantly, this 3D printing technology permits the creation of any complex and precisely defined concave

structure simply by changing the design or gradient of the inputted pattern (Figure S1). This feature represents a major advancement to previous 3D printing platforms, which rely on printing one dot or one layer at a time, while overcoming limitations associated with micromolding of soft biomaterials with complex designs.

A schemata of the 3D printing process at the molecular level is displayed in Figure 1b. For the first 15 layers, or masks, UV light is projected onto the entire prepolymer solution, photocrosslinking the base of the microwell structure. Subsequent optical masks with increasing areas of non-exposure (black, as indicated in Figure 1a) are displayed on the DMD. The concave hydrogel is therefore built in a continuous layer-by-layer fashion, alongside a continuously moving z-stage that coordinates its movements in the z direction with changes in the optical masks. Because we set the z-height to be 500 μm and there are 53 layers, the stage moves 9.4 μm for each layer, maintaining the same projection plane within the prepolymer solution as it moves through the layer series.

UV photopolymerization and gelation of PEGDA is a nonlinear process, where free radical initiation, polymer chain propagation, and termination take place on multi-order kinetics.^[22] Thus we sought to create a 3D printing process that allows for nonlinear UV exposure (see *Experimental*). Figure S2 depicts the changes to the nonlinear fabrication parameters as well as the outputted structure, maintaining the same gradient circle design throughout.

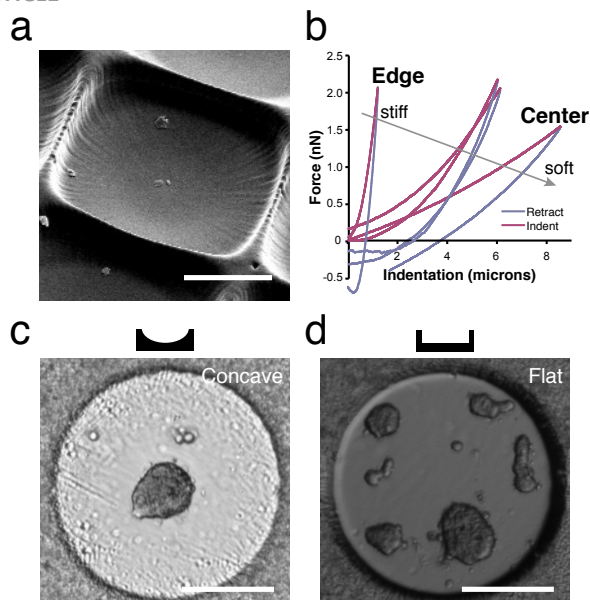


Figure 2. (a) Scanning Electron Microscopy image of dehydrated concave hydrogels. (b) AFM stiffness measurements at different regions of the concave hydrogel. The center of the well appears soft (10 Pa) and gradually increases in stiffness to the edge of the well (~200 Pa). The walls of the structure, which are also the tallest part and the most exposed to UV, have a stiffness of ~1-2 kPa. (c) Concave versus (d) flat hydrogels for tumor spheroid generation. Cell culture at the day 3 timepoint is displayed. All scale bars = 200 μm .

As T_0 decreases, the well shape becomes wider and less polymerized, and largely unpolymerized in the middle of the concave hydrogel (Figure S2a, panels *i* to *ii*). This lack of polymerization is presumably due to a lower exposure time for the 15 base layers, where the entire solution is exposed to UV light. We hypothesize that a longer exposure time to the base layers is required to generate free radicals for the rest of the structure. While increasing exposure to the base layers can be achieved by increasing T_0 in a linear fashion, this method overpolymerizes the remaining layers of the hydrogel structure allowing for an undefined shape that is not optically clear (Figure S2a, panel *i*). We thus modulated the nonlinear factor, A_2 , to vary the exposure time for each layer. When A_2 is negative, every successive layer is exposed for a shorter duration than the previous layer, in turn speeding up the entire fabrication process as it proceeds through the entire 53 layers (Figure S2a, panels *iii* to *v*). By increasing T_0 and making A_2 more negative, the bulk of the UV irradiation shifts to the earlier layers, allowing a longer duration for free radical generation in the base layers (where the entire prepolymer solution is exposed to UV light).

We empirically determined the optimal T_0 and A_2 values to be 0.95 s and -0.023, respectively, fitting our aforementioned

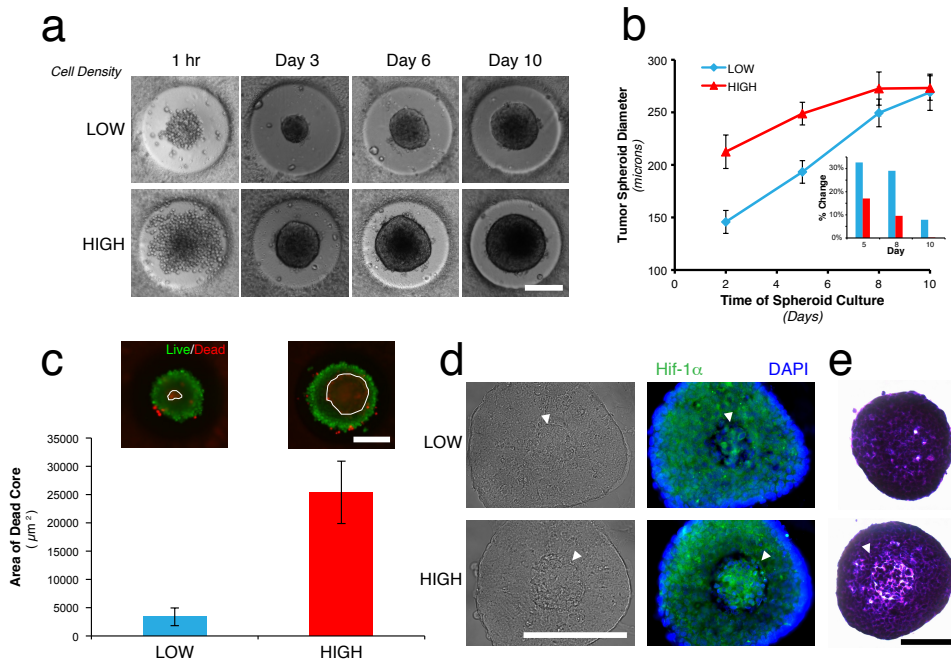
design criteria – that is, a an optically clear, concave hydrogel that permits single spheroid formation in its center (Figure S2a, panel *v*). Figure S2b provides a graphical understanding of the cumulative exposure time in accordance to the layers for each of the five cases shown in Figure S2a. It is interesting to note the cumulative exposure time for the first 15 base layers increases from 6.0 s for linear exposure to 10.2 s for nonlinear exposure in panels *ii* and *v* of Figure 2a, respectively (Figure 2b inset). Thus, we believe that a longer duration of UV exposure to the base layers is required to initiate the free radical polymerization process throughout the prepolymer solution. Below this time, we observed unpolymerized sections in the microwell center.

We used scanning electron microscopy to assess the topography of the hydrogels. (Figure 2a). The hydrogel displays a gradually increasing slope from the center to the edge and steep walls, indicating a concave shape. Atomic force microscopy was used to characterize the stiffness profile on the concave hydrogel surface (Figure 2b). The structure displayed a soft, low modulus center (10 Pa) that stiffened to the edge of the well (~200 Pa). The tallest part of the structure – the wall of the hydrogel – represented the stiffest region (1-2 kPa). We hypothesized that the soft center correlates to earlier layers of UV exposure during the fabrication process, and as it proceeds through the layers, increasing UV exposure drives additional crosslinking to stiffen the hydrogel. We confirmed this by taking stiffness measurements of flat hydrogel structures with different UV exposure to the base (Figure S3). It appears that the flat wells with 15 base layers has an average stiffness of 20 Pa, while 24 base layers and 34 base layers have higher moduli profiles of 151 Pa and 203 Pa, respectively. Thus, it is likely that the gradient UV exposure in our concave hydrogels is due to the variable light exposure in the continuous layer-by-layer 3D printing process.

For preliminary cell studies, we fabricated flat or concave hydrogels and seeded BT474 breast cancer cells to examine the effect of concavity on spheroid generation (Figure 2c and d). When flat hydrogels were used in cell culture, several spheroids of varying sizes formed within each well, while the desired single spheroid formation was achieved in the concave hydrogel microstructures. Expanding on our first cell experiments, BT474 breast cancer cells were seeded at various densities and used to assess tumor spheroid generation and growth within the concave hydrogels (Figure 3a). At day 2, LOW (250 k mL^{-1}) and HIGH (750 k mL^{-1}) cell seeding densities produced spheroids with diameters $146 \pm 11 \mu\text{m}$ and $213 \pm 16 \mu\text{m}$, respectively (Figure 3b). However, over the course of the next several days, spheroids from the HIGH group began to plateau at a size of around 250-275 μm , while the

Lab on a Chip

Figure 3. Concave hydrogels used for long-term 3D spheroid culture of two distinct models – breast cancer spheroids iPSC embryoid bodies. (a) Timelapse images of tumor spheroids grown at LOW (250 k mL⁻¹) and HIGH (750 k mL⁻¹) cell densities. (b) Tumor spheroid sizes quantified over 10 days for LOW and HIGH cell seeding density (n = 12 or more). Inset: percent change in spheroid size in relation to the previous timepoint. (c) Fluorescent images at day 10 depict live/dead staining (green/red), and the area of the dead core quantified (white outline of red fluorescence in live/dead images) (n=9). (d) Immunohistochemistry staining of HIF-1-alpha (hypoxia marker), DAPI (nuclear), and brightfield images of spheroid cross-sections. (e) Hematoxylin & Eosin (H&E) staining of spheroid cross-sections. Scale bars = 200 μ m.



smaller spheroids from the LOW group continued to grow in size, albeit smaller than the 250 μ m threshold. Growth rates for each group confirmed this trend (Figure 3b, inset). At day 10, spheroid diameters for both groups were within standard deviations of each other – 269 \pm 17 μ m and 273 \pm 12 μ m for LOW and HIGH groups, respectively.

Interestingly, live/dead staining with calcein AM/ethidium homodimer at day 10 showed that the HIGH group exhibited a 10-fold increase in its dead core area, compared to the LOW group: 25,394 \pm 5,514 μ m² and 3,385 \pm 1,565 μ m² for HIGH and LOW groups, respectively (Figure 3c). This observation suggests a necrotic core forming in the HIGH group, correlating with regression in spheroid growth. It has been well documented that tumor spheroids greater than \sim 200 μ m in diameter demonstrate a hypoxic core due to a nutrient and gas transport gradient, which in turn can lead to necrosis.^[9, 23] The presence of a hypoxic core in the tumor spheroid provides a more physiologically relevant tumor model for cancer screening applications, as tumor hypoxia *in vivo* drives a pro-angiogenic cascade for continued growth and invasion.^[24] Hypoxia was confirmed with immunostaining of the spheroid cross-sections for HIF-1 α , a biomarker for hypoxia (Figure 3d), and necrosis was observed in hematoxylin and eosin staining (Figure 3e). The spheroids showed considerable hypoxia and necrosis more prevalently in spheroids from the HIGH group. These data are in good agreement with previous literature regarding tumor spheroid progression (e.g. hypoxia and necrosis).

Human iPSCs were utilized in subsequent experiments for generating and culturing EBs. iPSCs, derived by retroviral transduction of a combination of four transcription factors,

Oct4, Sox2, c-Myc and Klf4, are stem cells with an equivalent self-renewal and differentiation capacity as embryonic stem cells.^[14] In addition to their pluripotency, iPSCs provide a superior platform for clinical translation because they are autologous by nature (patient-specific). This facilitates their use in personalized disease modeling, drug testing, and regenerative medicine development, as well as minimizing any ethical concerns.

iPSCs were seeded on top of the concave hydrogels at a density of 100 k mL⁻¹. Single EBs formed after three days of culture, with an average diameter of 155 \pm 17 μ m (Figure 4a). Flat microstructures, conversely, generated a broader distribution of EB sizes, such that an initial seeding density of 200 k mL⁻¹ produced EBs of 129 \pm 48 μ m. We reported similar observations for flat hydrogels with our breast cancer spheroids (Figure 2d). This is also consistent with previous literature on flat microwells that EBs only form at a critical cell density proportional to the microwell size, below which they form infrequently or at varied sizes.^[25] At day 3, EBs showed pluripotency by immunostaining for Nanog and Oct4, transcription factors highly expressed in embryonic stem cells (Figure 4b). Grown to day 10, EBs displayed morphological changes in their size, shape, and appearance in the form of intra-organoid cavities (Figure 4c and Figure S4). We hypothesized that this was due to spontaneous differentiation that can occur in these pluripotent cells, based on similar

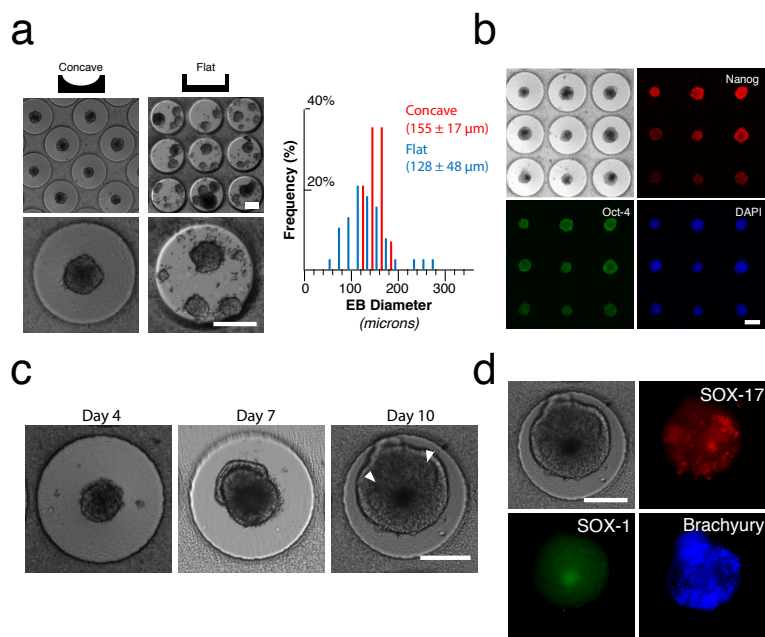


Figure 4. (a) Day 3 of human iPSC cells grown on either concave hydrogels (cell seeding density 100 k mL^{-1}) or flat hydrogels (cell seeding density $\sim 200 \text{ k mL}^{-1}$). Size distribution is quantified for each type ($n =$ at least 14 for each group). (b) Immunofluorescent staining of EBs on day 3 for Nanog and Oct4, two markers for pluripotency and non-differentiated cells, and DAPI, a nuclear stain. (c) brightfield images over longer timepoints (10 d), where white arrows indicate intra-organoid cavities. (d) Immunofluorescent staining at day 10 of the three germ layers – ectoderm (SOX-1), endoderm (SOX-17), and mesoderm (brachyury) in concave hydrogels (initial cell seeding density $\sim 100 \text{ k mL}^{-1}$). All scale bars = $200 \mu\text{m}$.

observations in the literature.^[5] Immunostaining confirmed EB differentiation to all three germ layers for both cell seeding densities, as evidenced by their co-expression of SOX-17 (endoderm), SOX-1 (ectoderm) and brachyury (mesoderm) (Figure 4d). These differentiation results serve to only show the possibility of visualizing differentiation of a single EB housed in the concave hydrogel. Further studies will be needed to address and quantify the different stages of embryogenesis and differentiation, as well as a more focused review on the necessary components in cell culture (e.g. media, growth factors) contributing to tissue-specific differentiation.^[4,26]

Conclusions

The concave hydrogel platform described here can be a valuable tool in the development of a multitude of spheroid-based cell culture models, especially for longer timepoints beyond the first media exchange. These may include tumor progression (e.g. proliferation, hypoxia, necrosis), migration and angiogenesis as well as various EB, and in particular iPSC, studies such as embryogenesis, organogenesis, toxicity, and patient-specific disease models. Due to its high reproducibility, low cost (material and time), ease of fabrication, and retention of the spheroids for long-term culture, this technology could also be adapted for high-throughput screening if individual hydrogel microstructures were to be printed into a high-throughput plate.

Acknowledgements

The project described was supported by grants EB012597 and EB017876 from the NIH-National Institute of Biomedical Imaging and Bioengineering and grant CMMI-1120795 from the National Science Foundation (SC); the Saving tiny Heart

Society and the California Institute of Regenerative Medicine (FS); ARRA grant (RC1 EB011780) from the NIH-National Institute of Biomedical Imaging and Bioengineering (KV); and DP020D006460 grant from the NIH (AJE). The authors would also like to thank John Warner for helpful discussions.

Notes and references

- ^a Department of NanoEngineering, University of California San Diego, 9500 Gilman Drive, La Jolla, CA 92093-0448, USA
- ^b Cancer Center, Sanford-Burnham Medical Research Institute, La Jolla, California, USA, 92037
- ^c Department of Bioengineering, University of California San Diego, 9500 Gilman Drive, La Jolla, CA 92093, USA
- ^d Materials Science and Engineering Program, University of California San Diego, 9500 Gilman Drive, La Jolla, CA 92093, USA
- ^e Department of Medicine (Cardiology Division), University of California San Diego, 9500 Gilman Drive, La Jolla, CA, 92093, USA
- ^f Sanford Consortium for Regenerative Medicine, La Jolla, CA, 92037, USA

Electronic Supplementary Information (ESI) available: details of experimental setup and supplementary figures. See DOI: 10.1039/b000000x/

- 1 D. Huh, G. A. Hamilton, D. E. Ingber, *Trends in cell biology*, 2011, **21**, 745.
- 2 N. T. Elliott, F. Yuan, *Journal of pharmaceutical sciences*, 2011, **100**, 59.
- 3 F. Pampaloni, E. G. Reynaud, E. H. Stelzer, *Nature reviews. Molecular cell biology*, 2007, **8**, 839.
- 4 Y. S. Hwang, B. G. Chung, D. Ortmann, N. Hattori, H. C. Moeller, A. Khademhosseini, *Proceedings of the National Academy of Sciences of the United States of America*, 2009, **106**, 16978.
- 5 J. Itskovitz-Eldor, M. Schuldiner, D. Karsenti, A. Eden, O. Yanuka, M. Amit, H. Soreq, N. Benvenisty, *Molecular medicine*, 2000, **6**, 88.

- 6 J. R. Spence, C. N. Mayhew, S. A. Rankin, M. F. Kuhar, J. E. Vallance, K. Tolle, E. E. Hoskins, V. V. Kalinichenko, S. I. Wells, A. M. Zorn, N. F. Shroyer, J. M. Wells, *Nature*, 2011, **470**, 105.
- 7 A. M. Laib, A. Bartol, A. Alajati, T. Korff, H. Weber, H. G. Augustin, *Nature protocols*, 2009, **4**, 1202.
- 8 J. M. Kelm, V. Djonov, L. M. Ittner, D. Fluri, W. Born, S. P. Hoerstrup, M. Fussenegger, *Tissue engineering*, 2006, **12**, 2151.
- 9 F. Hirschhaeuser, H. Menne, C. Dittfeld, J. West, W. Mueller-Klieser, L. A. Kunz Schughart, *Journal of biotechnology*, 2010, **148**, 3.
- 10 J. Fukuda, K. Nakazawa, *Tissue Eng*, 2005, **11**, 1254.
- 11 C. R. Thoma, S. Stroebel, N. Rosch, B. Calpe, W. Krek, J. M. Kelm, *Journal of biomolecular screening*, 2013, **18**, 1330.
- 12 Y. Y. Choi, B. G. Chung, D. H. Lee, A. Khademhosseini, J. H. Kim, S. H. Lee, *Biomaterials*, 2010, **31**, 4296.
- 13 G.S Jeong, J.H. Song, A.R. Kang, Y. Jun, J.H. Kim, J.Y. Chang, S.H. Lee, *Adv Healthc Mater*, 2013, **2**, 119.
- 14 H. C. Moeller, M. K. Mian, S. Shrivastava, B. G. Chung, A. Khademhosseini, *Biomaterials*, 2008, **29**, 752.
- 15 J. M. Karp, J. Yeh, G. Eng, J. Fukuda, J. Blumling, K. Y. Suh, J. Cheng, A. Mahdavi, J. Borenstein, R. Langer, A. Khademhosseini, *Lab on a chip*, 2007, **7**, 786.
- 16 M. D. Ungrin, C. Joshi, A. Nica, C. Bauwens, P. W. Zandstra, *PLoS one*, 2008, **3**, e1565.
- 17 N. A. Peppas, J. Z. Hilt, A. Khademhosseini, R. Langer, *Adv Mater*, 2006, **18**, 1345.
- 18 A.P. Zhang, X. Qu, P. Soman, K.C. Hribar, J.W. Lee, S.C. Chen, S. He, *Adv Mater* 2012, **24**, 4266.
- 19 Y. S. Choi, L. G. Vincent, A. R. Lee, K. C. Kretchmer, S. Chirasatitsin, M. K. Dobke, A. J. Engler, *Biomaterials*, 2012, **33**, 6943.
- 20 M. Radmacher, *Method Cell Biol*, 2007, **83**, 347.
- 21 K. C. Hribar, P. Soman, J. Warner, P. Chung, S. Chen, *Lab on a chip*, 2014, **14**, 268.
- 22 S. Kizilel, V.H. Perez-Luna, F. Teymour, *Macromol Theor Simul* 2006, **15**, 686.
- 23 G. Metha, A.Y. Hsiao, M. Ingram, G.D. Luker, S. Takayama, *J Control Release*, 2012, **164**, 192.
- 24 D. Shweiki, M. Neeman, A. Itin, E. Keshet, *Proceedings of the National Academy of Sciences of the United States of America*, 1995, **92**, 768.
- 25 K. Takahashi, K. Tanabe, M. Ohnuki, M. Narita, T. Ichisaka, K. Tomoda, S. Yamanaka, *Cell*, 2007, **131**, 861.
- 26 M. Schuldiner, O. Yanuka, J. Iskovitz-Eldor, D.A. Melton, N. Benvenisty, *Proceedings of the National Academy of Sciences of the United States of America*, 2000, **97**, 11307.